Measuring the Electron Inelastic Mean Free Path in Epitaxial Graphene on SiC

Mojtaba Amjadipour[1], Jennifer MacLeod[1], Josh Lipton-Duffin[2], Anton Tadich[3], John J Boeckl[4], Francesca Iacopi[5], and Nunzio Motta[1*]

[1] School of Chemistry, Physics and Mechanical Engineering, Science and Engineering Faculty, Queensland University of Technology, QLD, Australia

[2] Central Analytical Research Facility, Institute for Future Environments, Science and Engineering Faculty, Queensland University of Technology, QLD, Australia

[3] Australian Synchrotron, 800 Blackburn Road, Clayton, 3168 VIC, Australia

[4] Materials and Manufacturing Directorate, Air Force Research Laboratories, Wright-Patterson AFB, 45433 OH, United States of America

[5] School of ~~Computing and Communications~~Electrical and Data Engineering, Faculty of Engineering and Information Technology, University of Technology Sydney, NSW, Australia

Abstract

The inelastic mean free path (IMFP) for carbon-based materials is notoriously challenging to model, and moving from bulk materials to 2D materials may exacerbate this problem, making the measurement of IMFP in 2D carbon materials quite critical. We present an experimental measurement for IMFP in epitaxial graphene on SiC using photoelectron spectroscopy (PES) over an electron kinetic energy range of 50-1150 eV. The results suggest that the existing models for IMFP may not adequately capture the physics of electron interactions in 2D materials. Our experimental values exceed the theoretical predictions and experimental values of the IMFP in graphite for all energies through this range. We emphasize the significant effect of interface and demonstrate that the IMFP in the so-called 'buffer layer' is smaller than for free-standing graphene. Was this the first work of this kind? If so, need to make clear how/why in the abstract This work suggests that more work may need to be done, both experimentally and theoretically, to establish accurate IMFPs for graphene and for other 2D materials.

---

[*] Corresponding author.

1. Introduction

The average distance that electron moves through a material without undergoing an energy-loss scattering event is known as the inelastic mean free path (IMFP) [1]. Energy-loss events are caused primarily by electron-electron or electron-phonon scattering. Electron-electron scattering significantly depends on the kinetic energy, and therefore, in photoemission, these losses are proportional to the photoemission excitation energy. Conversely, electron-phonon scattering does not show any significant energy dependence and the losses are very low (~ 50 meV). As a result, for electrons with kinetic energy more than ~ 6 eV, energy loss due to electron-phonon scattering is negligible and electron-electron scattering dominates [2]. A precise understanding of IMFP for different materials is vital for a number of measurement techniques such as photoelectron spectroscopy (PES) [3], photoelectron diffraction [4], Auger electron spectroscopy [5], and electron microscopy [6].

IMFPs can be experimentally measured using low-energy electron diffraction (LEED) [7], X-ray absorption fine structure (XAFS) spectroscopy [8], and photoelectron spectroscopy (PES) [2]. A common approach for IMFP measurement is to grow or deposit a thin layer of one material on another and to investigate the peak intensity change of the substrate as a function of thickness of the deposited layer [9]. The accuracy of this method depends critically on having a precise understanding of the film thickness, and the homogeneity of the film and any possible contamination will strongly affect the extracted IMFP. Electron beam attenuation measurements also have been used for measuring IMFP for low energy ranges of 5-11 eV [10, 11].

Comprehensive theoretical models have been developed to predict the IMFP in a number of solids over a range of kinetic energies going from 50 eV to 200 keV [12-18]. A series of works by Tanuma et al report calculated IMFPs for a number of elements [12-15, 19-22]. These calculations rely on an algorithm developed by Penn [23] based on experimental optical data from synchrotron radiation studies [24], which relates the inelastic scattering probability to energy loss, and the Lindhard dielectric function, which describes the scattering probability as a function of momentum transfer. They also introduced an equation called Tanuma, Powell, and Penn (TPP-2M) to predict IMFP of electrons in different compounds and elemental solids at 50-2000 eV energy range [25].

The parameters in TPP-2M model can be derived from material properties such as density, atomic weight, and number of valence electrons per atom [19, 25].

In recent years graphene has emerged at the vanguard of materials due to its extraordinary properties [26-30]. It has been the subject of many electron-collection-based studies such as PES, LEED, Auger electron spectroscopy and electron microscopy [29, 31-34]. Thus, having a clear understanding of the electron IMFP is crucial for accurate data interpretation and analysis. However, the IMFP of carbon polymorphs has consistently been difficult to model; this challenge has been recognized for decades and remains an outstanding challenge [12-15, 19]. Tanuma et al experimentally measured IMFP for graphite using elastic-peak electron spectroscopy (EPES), and found the experimental data to be about 50% higher than their theoretical predictions [35]. Characterizing the IMFP is even more challenging for graphene compared to graphite as interface effect will dominate and anisotropies are magnified [14]. Very little is known about how IMFPs vary in moving from bulk to 2D materials [32], and this represents an emerging challenge for the burgeoning field of 2D materials, since accurate materials characterization requires a good understanding of IMFP.

Here we present a measurement of the IMFP in epitaxial graphene fabricated on SiC using synchrotron PES, and supported by thickness measurements using transmission electron microscopy (TEM). Our experiments are performed in ultra-high vacuum (UHV) chamber without being exposed to air which eliminates any chance of contamination significantly. Graphene growth using high temperature annealing of SiC is an attractive approach for device fabrication because it does not require a transfer step, which can adversely affect the properties of the graphene [36-38]. Epitaxial graphene growth on SiC creates a buffer layer at the interface between the graphene and the SiC; this layer is a graphene-like layer that is partially bound to the substrate [39, 40]. The buffer layer can be eliminated using a hydrogen intercalation process that cleaves the bonds to the surfaces and returns it to a graphene bonding configuration [34, 41].We demonstrate the effect of the buffer layer in IMFP and compare it to free-standing graphene on SiC produced by hydrogen intercalation. We found that the electrons IMFP is shorter in the buffer layer compared to a free-standing graphene layer.

2. Experimental Details

A 1 µm thick 3C-SiC(111) layer grown on Si(111) was obtained from NOVASIC (France). The SiC/Si(111) wafer was chemically and mechanically polished to the surface roughness of ~ 1 nm (StepSiC® by NOVASIC (France)) [42]. Each sample was cleaned by successive 10 minutes sonication in acetone, isopropanol and deionised water, respectively.

Synchrotron-based PES measurements were conducted at the soft X-ray beamline of the Australian Synchrotron. Samples were annealed at 400 °C for several hours to remove contaminants. Temperature measurements were made using an optical pyrometer (IRCON Ultimax UX-20P with emissivity = 0.9). A SPECS Phoibos 150 hemispherical analyser operating at a pass energy of 10 eV was used for PES measurements.

Atomic hydrogen exposure was achieved using EFM-H atomic hydrogen source (FOCUS GmbH) operating at an apparent chamber pressure of ~ 5×10^{-6} mbar and 40 W power. Atomic hydrogen etching assists with elimination of contamination and improving the flatness of the SiC surface, and has been routinely employed as a preparation step prior to graphene fabrication [43-45].

The epitaxial graphene fabrication involves annealing at 1200 - 1250 °C for 5 - 10 minutes. The thickness of the resultant graphene layer depends on annealing time and temperature, with longer and hotter anneal cycles producing larger numbers of graphene layers [31, 46]. An FEI Tecnai F30 TEM system operating at 200 keV was used for graphene layer thickness measurements. TEM sample preparation was conducted by lift out procedure using a FEI Strata DB235 FIB/SEM system.

3. Results and Discussions

Core-level PES of Si 2p using a photon energy of 1253 eV are presented in Fig. 1. The measurement was conducted first on the reference SiC/Si(111) sample and then on the sample covered with graphene. The intensity (the area under the peak) decreases for the graphene/SiC sample (I) compared to the reference sample (I_0). This is because for the sample with the graphene layer, electrons originating in the SiC must travel through the graphene layer which results in additional scattering and energy loss events, and these electrons are no longer detected at the

expected energy for the Si 2p core level. We use this intensity loss to calculate the IMFP in epitaxial graphene.
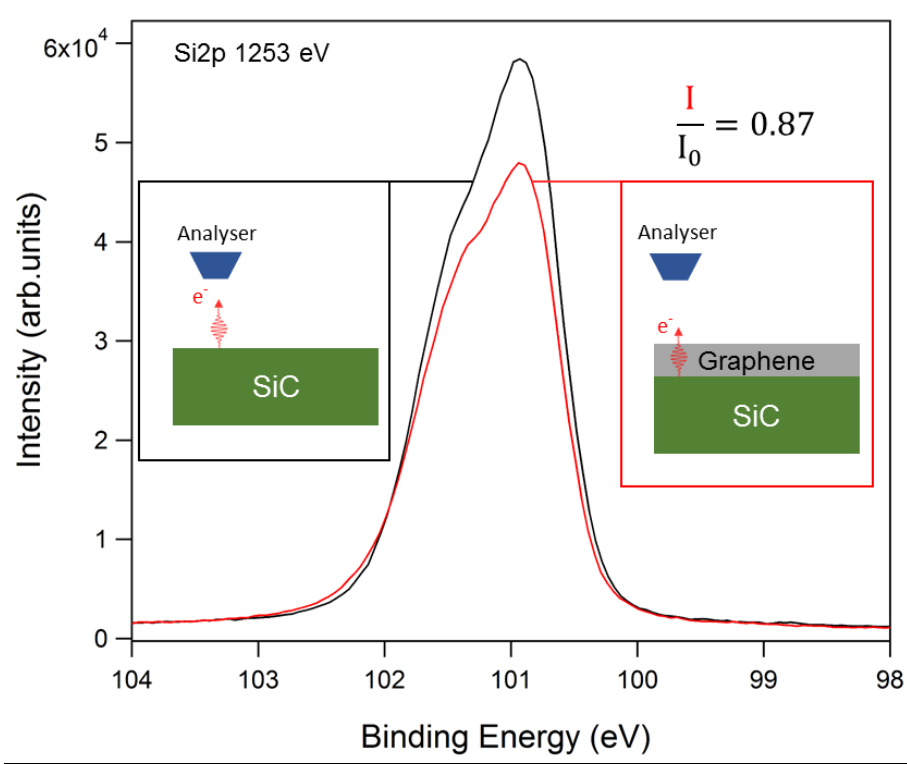

Fig. 1 Si 2p spectra for the SiC reference sample and the graphene/SiC sample indicating the intensity decrease.

Fig. 2 shows the intensity variation with photon energy for Si 2p and C1s spectra of the graphene/SiC sample, acquired over photon energies from 150-1253 eV (Si 2p) and 330-1253 eV (C 1s). From the C 1s spectrum it is clear that higher photon energies produce more substrate-related (SiC substrate) signal whereas lower energies enhance the surface-related (graphene/buffer layer) signal (Fig. 2a). To calculate the IMFP for electrons inside the epitaxial graphene layer, we studied the Si 2p signal as this is generated almost exclusively from the SiC substrate (Fig. 2b). The intensity change (a.k.a. Transmission, I/I_0) with photon energy of the Si 2p peak for graphene/SiC is reported in the supplementary information in Table S1 and Fig. S1.
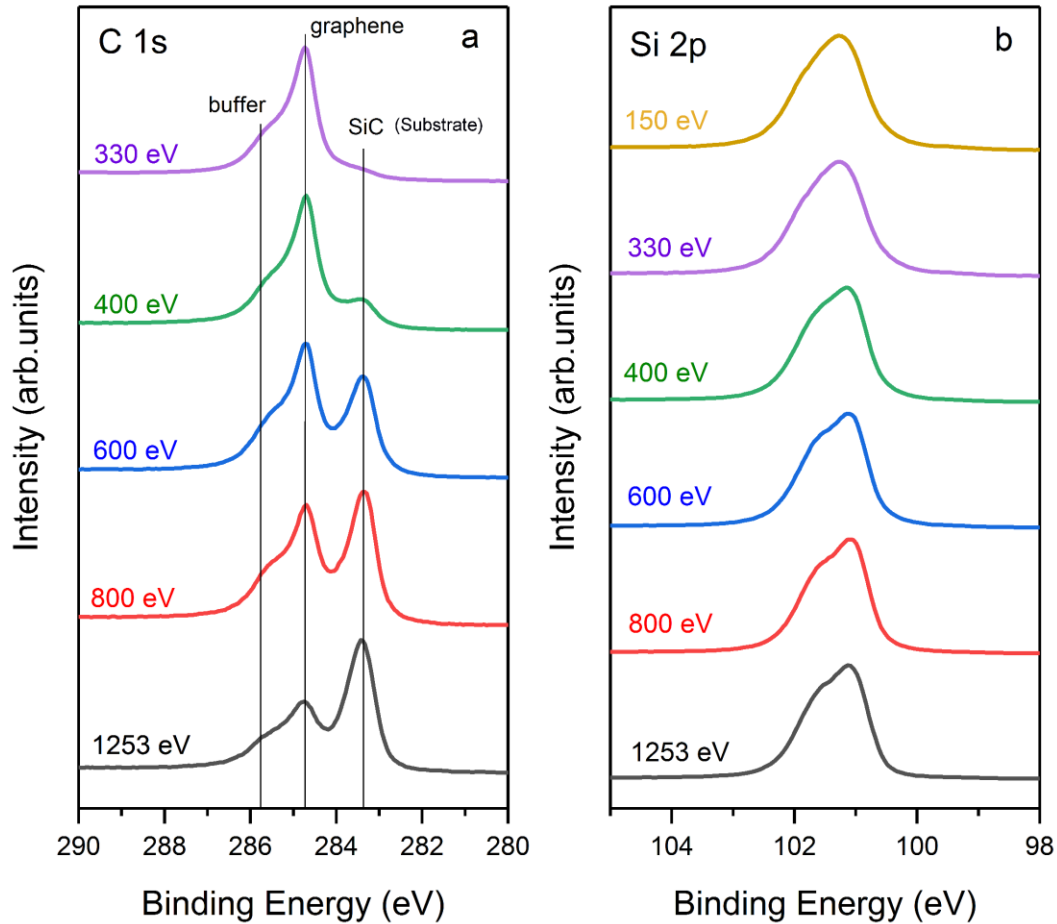
Fig. 2 PES spectrum of graphene/SiC measured with different photon energies, (a) C 1s and (b) Si 2p.

By studying the intensity changes as a function of kinetic energy one can calculate the IMFP of electrons in the graphene layer. The attenuation of a low-energy electron signal can be expressed as:

$$\frac{I}{I_0} = e^{-\frac{t}{\lambda}},$$

where I is the intensity of the SiC component with graphene on top, I_0 is the intensity of the bare SiC component as the reference sample, t is the thickness of the graphene layer in nm, and λ is the IMFP in nm. The thickness of the graphene layer was measured directly by TEM of the sectioned sample, which indicates two graphene-like layers on the SiC substrate (Fig 3). The first layer on the substrate is commonly called buffer layer as it is partially bonded to the substrate (inset of Fig. 3); the presence of the buffer layer is confirmed by PES data (Fig. 2a and S2). The

thickness of the graphene 'film' is thus 0.6 nm, corresponding to one graphene layer plus the buffer layer (Fig. 3 inset). Based on this measured thickness of graphene layer on the SiC substrate, the IMFP was calculated at six different energies from the intensity attenuation equation above.
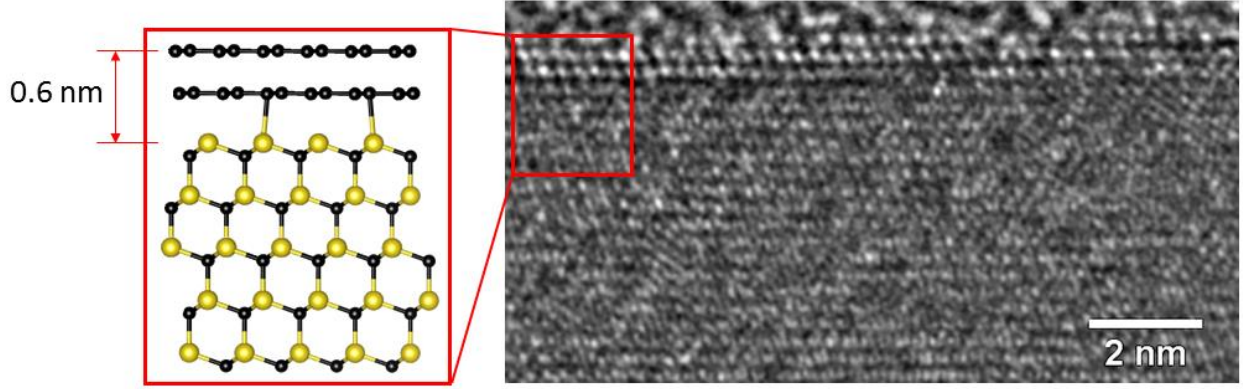

Fig. 3 TEM image showing that the sample has the coverage of two graphene like layers (first layer corresponds to the buffer layer and the second one is graphene supported by the PES data).

The IMFP is plotted in Fig. 4. In order to fit this data a modified Bethe equation [20] introduced by Tanuma et al [22] was employed, whereby:

$$\lambda = \frac{E}{E_p^2[\beta \ln(\gamma E) - \left(\frac{C}{E}\right) + \left(\frac{D}{E^2}\right)]}$$

where λ is the electron IMFP (nm), E is the electron energy (eV), E_p is the free-electron plasmon energy (eV) (for carbon $E_p = 22.3$ eV). β, γ, C and D are constant parameters of the equation [22]. Our fit parameters can be found in the supporting information Table S2. In addition to the measured IMFP for graphene in the present work, other reported values for graphite and graphene are shown in Fig. 4. The calculated values for graphite using optical data are reported by Shinotsuka et al [13] and the TPP-2M model prediction for graphite is included [15]. Also, the IMFP measured by Xu et al [32] using Auger electron spectroscopy (50-500 eV) for CVD grown graphene and transferred to a SiO_2 substrate is shown in the figure.
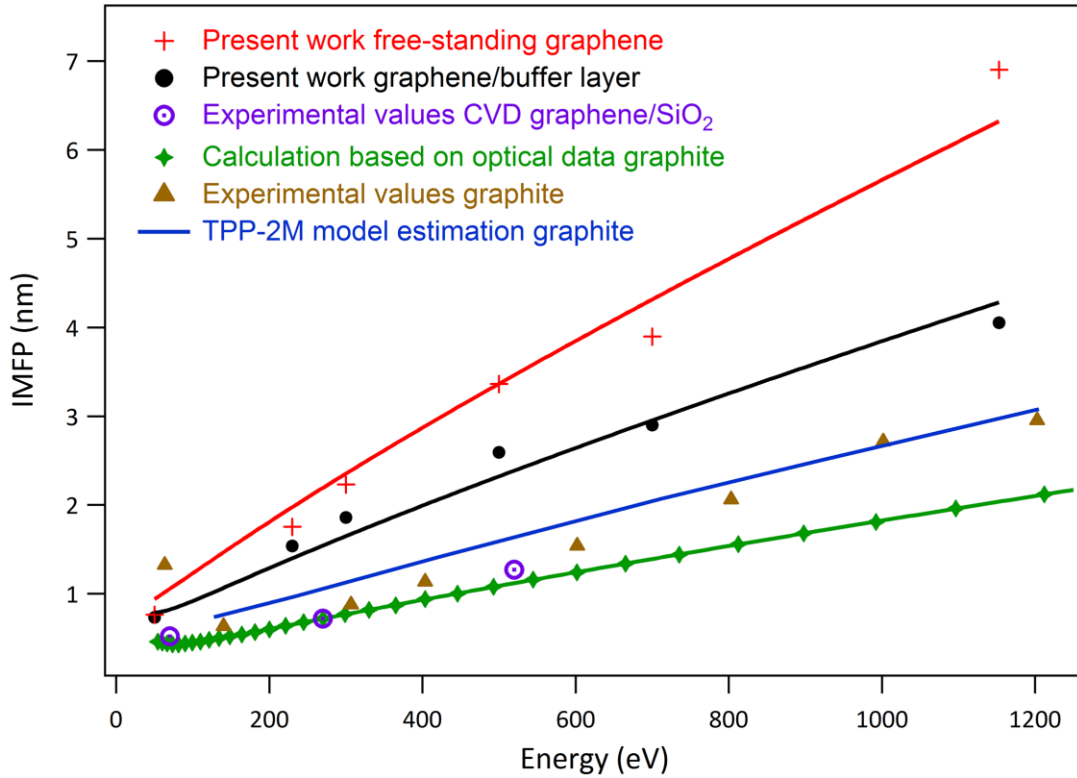
Fig. 4 IMFP measured in the present work for graphene/buffer layer and free-standing graphene compared with the computational values based on optical data for graphite [13] and TPP-2M model prediction for graphite [15]. Experimental values reported for graphite by Tanuma et al [35] and CVD graphene transferred to SiO_2 substrate by Xu et al [32]. The solid lines represent the fitting of the data using the modified Beth equation [22].

We find that our experimental IMFPs for graphene on SiC are approximately double the reported theoretical values for graphite [13], and about 50% higher than experimental values for graphite measured using EPES [35] and predicted values by TPP-2M equation [15]. The Penn algorithm does not account for sample anisotropy, and this was suggested as the main reason for observing such significant variation between experimental values and the theoretical calculation results for graphite [14]. TPP-2M model can describe the experimental values for graphite much better, but still under predicts the values found here for graphene [15]. Interface effects and the strong anisotropy of graphene may account for the variation between experimental values for graphite and present results for graphene.

Our data are approximately double of the values reported by Xu et al [32]. They studied the IMFP in CVD grown graphene transferred to SiO_2/Si substrate using Auger electron spectroscopy in 50-500 eV energy range, and used Raman spectroscopy to approximate the thickness of the graphene. This variation could stem from the presence of residue from the transfer process which would result in attenuation of electrons and an underestimation of the IMFP for graphene. Different techniques used for thickness measurement may affect the results. Xu et al also report that they neglected the attenuation in the outermost layer of graphene in their calculations, as well as in the SiO_2 layer, which could also contribute to this difference [32]. They indicated that their data derived from oxygen spectrum for monolayer graphene did not match with their other measurements which they attributed to interface diffraction and the two-dimensional nature of graphene [32].

To discern the effect of the buffer layer on the mean free path, we repeated the measurements after hydrogen intercalation of the graphene layer. The intercalation process breaks the bonds between the buffer layer and the SiC substrate and converts it to a complete graphene layer [34]. Hence our original sample, monolayer graphene with a buffer layer, is converted to a bilayer free-standing graphene on SiC as a result of the hydrogen intercalation (supporting information Fig. S3). Comparing the extracted IMFP in the free-standing bilayer graphene (red crosses) to the one with buffer layer (black dots) in Fig 4, it can be noted that IMFP for the free-standing graphene increase by about 30%. As the two layers have approximately the same thickness [47], we can conclude that the buffer layer scatters electrons substantially more than a free-standing graphene layer. This effect is likely due to the presence of sp^3 bonds between the buffer layer and the SiC substrate, which increases the scattering probability of electrons crossing the buffer layer compared to the free standing graphene layer. This is also observable in the C 1s PES spectra where the substrate-related peak intensity increases after hydrogen intercalation indicating that more electrons can travel through the graphene layer in the free-standing graphene compared to the buffer layer (supporting information Fig. S3).

Finally, we note that surface/volume considerations may mean that the measured values of the IMFP for graphene will depend critically on the thickness of the graphene layer, so that measurements from a bilayer graphene (present work) may not linearly extrapolate to thicker graphene layers. In this context, it may be reasonable to assume quite different behaviour between IMFPs in monolayer/bilayer graphene and bulk graphite. Such a disparity would mean that the

theoretical constructs established for bulk materials are unlikely to capture the physics associated with the IMFP in thin films, where interface/anisotropy effects are expected to be significant.

4. Conclusions

Using synchrotron PES in the energy range 50-1150 eV we have measured the IMFP of electrons in epitaxial graphene on SiC. We find that previous theoretical and experimental work for graphite under-predicts the absolute value of IMFP for graphene, while the energy dependence is very similar. By hydrogen intercalating the graphene, we demonstrated that the backbonded buffer layer scatters electrons more than a graphene layer. 2D materials such as graphene obey different physics than bulk materials. Surface and anisotropy effects are significant in 2D materials, and these are not captured in the current models for IMFP. This work highlights the need for more research into measuring the IMFP in 2D materials. In particular, measurements are required using a variety of methods, and on a range of different thicknesses and types of graphene (epitaxial, CVD, etc.) due to the presumed significant effect of the interface.

Acknowledgments

References

1. C. J. Powell and A. Jablonski, *Surface sensitivity of X-ray photoelectron spectroscopy.* Nuclear Instruments and Methods in Physics Research Section A: Accelerators, Spectrometers, Detectors and Associated Equipment, 2009. **601**(1): p. 54-65.
2. I. Lindau and W. E. Spicer, *The probing depth in photoemission and auger-electron spectroscopy.* Journal of Electron Spectroscopy and Related Phenomena, 1974. **3**(5): p. 409-413.
3. P. Cumpson, *Elastic scattering corrections in AES and XPS. III. Behaviour of electron transport mean free path in solids for kinetic energies in the range 100 eV< E< 400 eV.* Surface and interface analysis, 1997. **25**(6): p. 447-453.

4. F. Hillebrecht, H. Rose, T. Kinoshita, Y. Idzerda, G. van der Laan, R. Denecke, et al., *Photoelectron diffraction in magnetic linear dichroism.* Physical Review Letters, 1995. **75**(15): p. 2883.

5. W. S. M. Werner, W. Smekal, H. Störi, H. Winter, G. Stefani, A. Ruocco, et al., *Emission-Depth-Selective Auger Photoelectron Coincidence Spectroscopy.* Physical Review Letters, 2005. **94**(3): p. 038302.

6. K. Kimoto, T. Asaka, T. Nagai, M. Saito, Y. Matsui, and K. Ishizuka, *Element-selective imaging of atomic columns in a crystal using STEM and EELS.* Nature, 2007. **450**: p. 702.

7. J. Rundgren, *Electron inelastic mean free path, electron attenuation length, and low-energy electron-diffraction theory.* Physical Review B, 1999. **59**(7): p. 5106-5114.

8. C. T. Chantler and J. D. Bourke, *X-ray Spectroscopic Measurement of Photoelectron Inelastic Mean Free Paths in Molybdenum.* The Journal of Physical Chemistry Letters, 2010. **1**(15): p. 2422-2427.

9. P. W. Palmberg and T. N. Rhodin, *Auger Electron Spectroscopy of fcc Metal Surfaces.* Journal of Applied Physics, 1968. **39**(5): p. 2425-2432.

10. H. Kanter, *Slow-Electron Mean Free Paths in Aluminum, Silver, and Gold.* Physical Review B, 1970. **1**(2): p. 522-536.

11. S. M. Sze, J. L. Moll, and T. Sugano, *Range-energy relation of hot electrons in gold.* Solid-State Electronics, 1964. **7**(7): p. 509-523.

12. S. Tanuma, C. J. Powell, and D. R. Penn, *Calculations of electron inelastic mean free paths for 31 materials.* Surface and interface analysis, 1988. **11**(11): p. 577-589.

13. H. Shinotsuka, S. Tanuma, C. Powell, and D. Penn, *Calculations of electron inelastic mean free paths. X. Data for 41 elemental solids over the 50 eV to 200 keV range with the relativistic full Penn algorithm.* Surface and interface analysis, 2015. **47**(9): p. 871-888.

14. S. Tanuma, C. J. Powell, and D. R. Penn, *Calculations of electron inelastic mean free paths. IX. Data for 41 elemental solids over the 50 eV to 30 keV range.* Surface and interface analysis, 2011. **43**(3): p. 689-713.

15. S. Tanuma, C. J. Powell, and D. R. Penn, *Calculations of electron inelastic mean free paths.* Surface and interface analysis, 2005. **37**(1): p. 1-14.

16. H. T. Nguyen-Truong, *Low-energy electron inelastic mean free path in materials.* Applied physics letters, 2016. **108**(17): p. 172901.

17. H. T. Nguyen-Truong, *Analytical Formula for High-Energy Electron Inelastic Mean Free Path.* The Journal of Physical Chemistry C, 2015. **119**(41): p. 23627-23631.

18. W. S. M. Werner, K. Glantschnig, and C. Ambrosch-Draxl, *Optical Constants and Inelastic Electron-Scattering Data for 17 Elemental Metals.* Journal of Physical and Chemical Reference Data, 2009. **38**(4): p. 1013-1092.

19. S. Tanuma, C. J. Powell, and D. R. Penn, *Calculations of electron inelastic mean free paths.* Surface and interface analysis, 1994. **21**(3): p. 165-176.

20. H. Bethe, *Zur Theorie des Durchgangs schneller Korpuskularstrahlen durch Materie.* Annalen der Physik, 1930. **397**(3): p. 325-400.

21. S. Tanuma, C. J. Powell, and D. R. Penn, *Calculations of electron inelastic mean free paths. III. Data for 15 inorganic compounds over the 50–2000 eV range.* Surface and interface analysis, 1991. **17**(13): p. 927-939.

22. S. Tanuma, C. J. Powell, and D. R. Penn, *Calculations of electorn inelastic mean free paths. II. Data for 27 elements over the 50–2000 eV range.* Surface and interface analysis, 1991. **17**(13): p. 911-926.

23. D. R. Penn, *Electron mean-free-path calculations using a model dielectric function.* Physical Review B, 1987. **35**(2): p. 482-486.

24. H. J. Hagemann, W. Gudat, and C. Kunz, *Optical constants from the far infrared to the x-ray region: Mg, Al, Cu, Ag, Au, Bi, C, and Al2O3.* Journal of the Optical Society of America, 1975. **65**(6): p. 742-744.

25. S. Tanuma, C. J. Powell, and D. R. Penn, *Calculations of Electron Inelastic Mean Free Paths (IMFPs) VI. Analysis of the Gries Inelastic Scattering Model and Predictive IMFP Equation.* Surface and interface analysis, 1997. **25**(1): p. 25-35.

26. A. K. Geim, and Konstantin S. Novoselov., *The rise of graphene.* Nature materials, 2007. **6**(3): p. 183-191.

27. A. H. Castro Neto, F. Guinea, N. M. R. Peres, K. S. Novoselov, and A. K. Geim, *The electronic properties of graphene.* Reviews of Modern Physics, 2009. **81**(1): p. 109-162.

28. V. Y. Aristov, G. Urbanik, K. Kummer, D. V. Vyalikh, O. V. Molodtsova, A. B. Preobrajenski, et al., *Graphene synthesis on cubic SiC/Si wafers. Perspectives for mass production of graphene-based electronic devices.* Nano letters, 2010. **10**(3): p. 992-995.

29. C. Berger, Z. Song, X. Li, X. Wu, N. Brown, C. Naud, et al., *Electronic confinement and coherence in patterned epitaxial graphene.* Science, 2006. **312**(5777): p. 1191-1196.

30. Q. Wang, R. Kitaura, S. Suzuki, Y. Miyauchi, K. Matsuda, Y. Yamamoto, et al., *Fabrication and In Situ Transmission Electron Microscope Characterization of Freestanding Graphene Nanoribbon Devices.* Acs Nano, 2016.

31. B. Gupta, Notarianni, M., Mishra, N., Shafiei, M., Iacopi, F., & Motta, N., *Evolution of epitaxial graphene layers on 3C SiC/Si (111) as a function of annealing temperature in UHV.* Carbon, 2014. **68**: p. 563-572.

32. M. Xu, D. Fujita, J. Gao, and N. Hanagata, *Auger Electron Spectroscopy: A Rational Method for Determining Thickness of Graphene Films.* Acs Nano, 2010. **4**(5): p. 2937-2945.

33. E. Rollings, G.-H. Gweon, S. Zhou, B. Mun, J. McChesney, B. Hussain, et al., *Synthesis and characterization of atomically thin graphite films on a silicon carbide substrate.* Journal of Physics and Chemistry of Solids, 2006. **67**(9): p. 2172-2177.

34. M. Amjadipour, A. Tadich, J. J. Boeckl, J. Lipton-Duffin, J. MacLeod, F. Iacopi, et al., *Quasi free-standing epitaxial graphene fabrication on 3C–SiC/Si(111).* Nanotechnology, 2018. **29**(14): p. 145601.

35. S. Tanuma, T. Shiratori, T. Kimura, K. Goto, S. Ichimura, and C. J. Powell, *Experimental determination of electron inelastic mean free paths in 13 elemental solids in the 50 to 5000 eV energy range by elastic-peak electron spectroscopy.* Surface and interface analysis, 2005. **37**(11): p. 833-845.

36. A. Van Bommel, J. Crombeen, and A. Van Tooren, *LEED and Auger electron observations of the SiC (0001) surface.* Surface Science, 1975. **48**(2): p. 463-472.

37. M. Suemitsu, Y. Miyamoto, H. Handa, and A. Konno, *Graphene formation on a 3C-SiC (111) thin film grown on Si (110) substrate.* e-Journal of Surface Science and Nanotechnology, 2009. **7**: p. 311-313.

38. A. Ouerghi, A. Kahouli, D. Lucot, M. Portail, L. Travers, J. Gierak, et al., *Epitaxial graphene on cubic SiC (111)/Si (111) substrate.* Applied physics letters, 2010. **96**(19): p. 191910.

39. S. Goler, C. Coletti, V. Piazza, P. Pingue, F. Colangelo, V. Pellegrini, et al., *Revealing the atomic structure of the buffer layer between SiC(0001) and epitaxial graphene.* Carbon, 2013. **51**: p. 249-254.

40. B. Gupta, E. Placidi, C. Hogan, N. Mishra, F. Iacopi, and N. Motta, *The transition from 3C SiC (111) to graphene captured by Ultra High Vacuum Scanning Tunneling Microscopy.* Carbon, 2015. **91**: p. 378-385.

41. C. Riedl, C. Coletti, T. Iwasaki, A. A. Zakharov, and U. Starke, *Quasi-Free-Standing Epitaxial Graphene on SiC Obtained by Hydrogen Intercalation.* Physical Review Letters, 2009. **103**(24): p. 246804.

42. B. Gupta, I. Di Bernardo, P. Mondelli, A. Della Pia, M. G. Betti, F. Iacopi, et al., *Effect of substrate polishing on the growth of graphene on 3C–SiC (111)/Si (111) by high temperature annealing.* Nanotechnology, 2016. **27**(18): p. 185601.

43. A. Sandin, J. J. Rowe, and D. B. Dougherty, *Improved graphene growth in UHV: Pit-free surfaces by selective Si etching of SiC (0001)–Si with atomic hydrogen.* Surface Science, 2013. **611**: p. 25-31.

44. M. Amjadipour, M. MacLeod, J. Lipton-Duffin, F. Iacopi, and N. Motta, *Epitaxial graphene growth on FIB patterned 3C-SiC nanostructures on Si (111): reducing milling damage.* Nanotechnology, 2017. **28**(34): p. 345602.

45. P. Mondelli, B. Gupta, M. G. Betti, C. Mariani, J. L. Duffin, and N. Motta, *High quality epitaxial graphene by hydrogen-etching of 3C-SiC (111) thin-film on Si (111).* Nanotechnology, 2017. **28**(11): p. 115601.

46. F. Zarotti, B. Gupta, F. Iacopi, A. Sgarlata, M. Tomellini, and N. Motta, *Time evolution of graphene growth on SiC as a function of annealing temperature.* Carbon, 2016. **98**: p. 307-312.

47. W. Norimatsu and M. Kusunoki, *Structural features of epitaxial graphene on SiC {0? 0? 0? 1} surfaces.* Journal of Physics D: Applied Physics, 2014. **47**(9): p. 094017.

Supporting Information

Measuring the Electron Inelastic Mean Free Path in Epitaxial Graphene on SiC

Mojtaba Amjadipour[1], Jennifer MacLeod[1], Josh Lipton-Duffin[2], Anton Tadich[3], John J Boeckl[4], Francesca Iacopi[5], and Nunzio Motta[12]

[1] School of Chemistry, Physics and Mechanical Engineering, Science and Engineering Faculty, Queensland University of Technology, QLD, Australia

[2] Central Analytical Research Facility, Institute for Future Environments, Science and Engineering Faculty, Queensland University of Technology, QLD, Australia

[3] Australian Synchrotron, 800 Blackburn Road, Clayton, 3168 VIC, Australia

[4] Materials and Manufacturing Directorate, Air Force Research Laboratories, Wright-Patterson AFB, 45433 OH, United States of America

[5] School of ~~Computing and Communications~~Electrical and Data Engineering, Faculty of Engineering and Information Technology, University of Technology Sydney, NSW, Australia
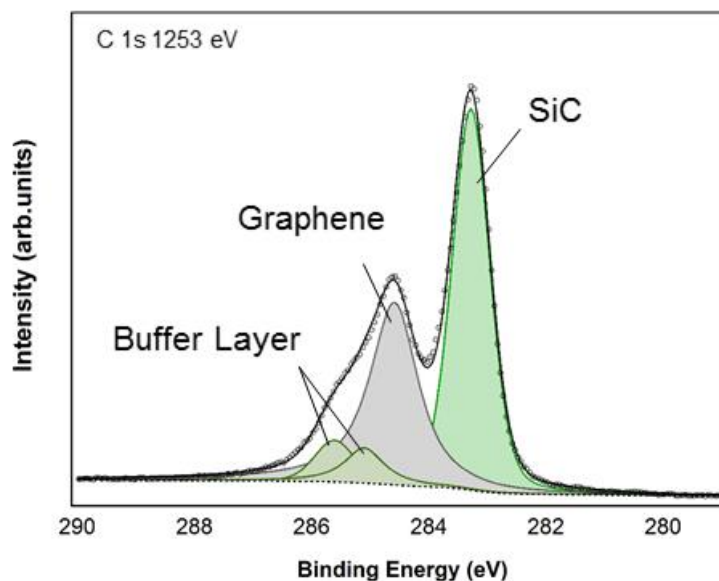
Fig. S 1. C 1s spectra of (a) graphene/SiC sample with buffer layer and (b) free-standing graphene on SiC produced by hydrogen intercalation process.

[2] Corresponding author.

Table 1. Si 2p peak intensity change for the sample covered with the graphene layer (I) and the reference sample (I_0).

Electron energy	I_0 (a.u.)	Error (%) I_0	I (a.u.)	Error (%) I	Transmission I/I_0
1151	70699.1	0.18	60970.3	0.20	0.86
698	278147	0.17	226175	0.20	0.81
498	647245	0.13	513497	0.16	0.79
298	1436070	0.11	1040180	0.13	0.72
228	1184090	0.17	801872	0.25	0.68
48	4506550	0.07	1986820	0.13	0.44

Table 2. Constant parameters of the modified version of the Bethe equation calculated for the fittings in Fig. 4.

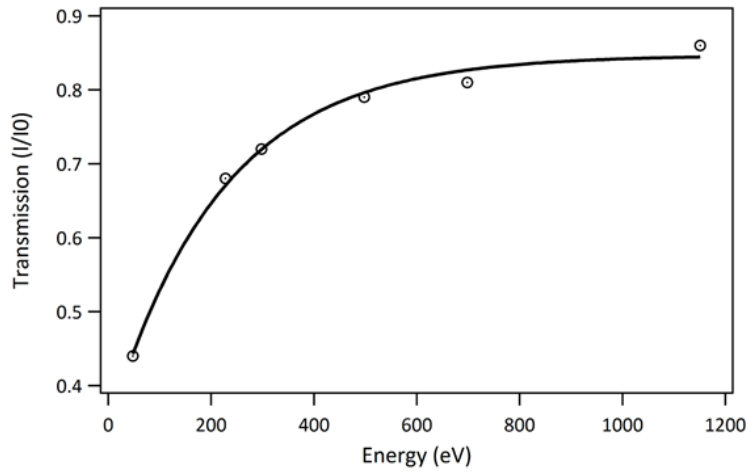| Condition	β (eV^{-1}nm^{-1})	γ (eV^{-1})	C (nm^{-1})	D (eVnm^{-1})
Present work - Graphene	0.13	0.06	1.44	40.00
Present work – Free-Standing Graphene	0.08	0.09	1.30	40.00
Shinotsuka - Graphite	0.237	0.109	14.572	235.190
Shinotsuka – C Glassy	0.158	0.118	9.520	206.350

Fig. S 2. Transmission (I/I0) as a function of the electron kinetic energy.
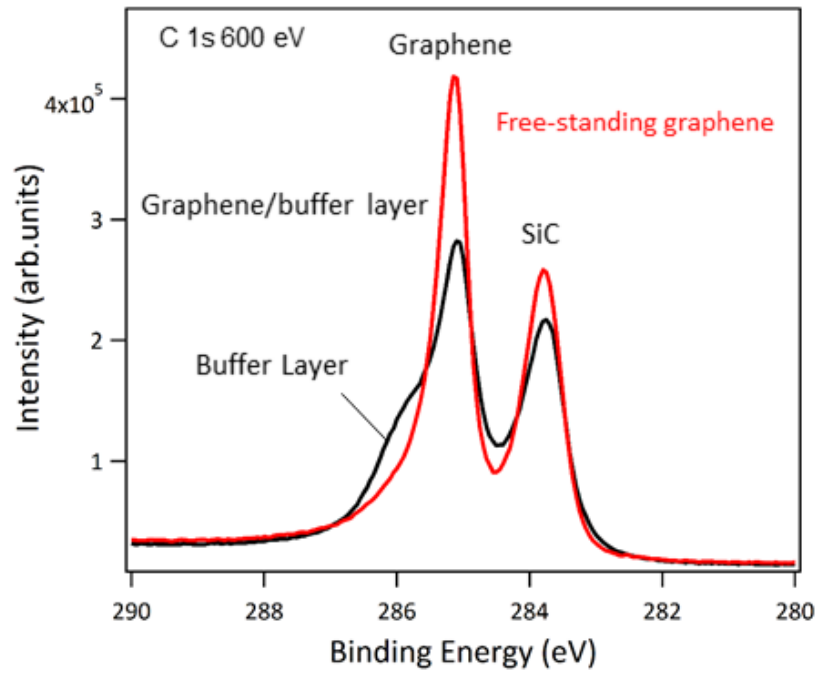
Fig. S 3. PES spectra of C 1s showing the elimination of the buffer layer components after hydrogen intercalation process and fabrication of the free-standing graphene.